

G. CENNINI<sup>✉</sup>  
G. RITT  
C. GECKELER  
M. WEITZ

# Bose–Einstein condensation in a CO<sub>2</sub>-laser optical dipole trap

Physikalisches Institut der Universität Tübingen, Auf der Morgenstelle 14, 72076 Tübingen, Germany

Received: 11 August 2003

Published online: 14 November 2003 • © Springer-Verlag 2003

**ABSTRACT** We report the achievement of Bose–Einstein condensation of a dilute atomic gas based on trapping atoms in tightly confining CO<sub>2</sub>-laser dipole potentials. Quantum degeneracy of rubidium atoms is reached by direct evaporative cooling in both crossed- and single-beam trapping geometries. At the heart of these all-optical condensation experiments is the ability to obtain high initial atomic densities in quasi-static dipole traps by laser-cooling techniques. Finally, we demonstrate the formation of a condensate in a field-insensitive  $m_F = 0$  spin projection only, which suppresses fluctuations of the chemical potential from stray magnetic fields.

PACS 03.75.Fi; 32.80.Pj; 42.50.Yk

## 1 Introduction

Since the first observation of Bose–Einstein condensation (BEC) in a dilute atomic gas, we have been witnessing dramatic progress in both theoretical and experimental studies of degenerate quantum gases [1, 2]. A variety of static and dynamic properties of the condensed, trapped atoms have been exploited [3]. Interference studies with Bose condensates have experimentally demonstrated the coherence properties expected for such a ‘giant matter wave’ [2]. More recently, the Mott-insulator phase transition has been observed by loading a magnetically trapped condensate into a steep optical lattice [4].

The standard approach for producing a Bose–Einstein condensate involves laser cooling of the atomic sample to a phase space density of  $10^{-6}$ , after which atoms in weak-field-seeking states are transferred into a magnetic trap [1, 2]. Further cooling proceeds by a radiofrequency field selectively transferring the most energetic atoms into untrapped states, which evaporatively cools the atoms to quantum degeneracy. A drawback of magnetic traps is that they only confine weak-field-seeking spins states, which, e.g., prevents one from studying spinor condensates directly in these traps [2]. Moreover, atoms in field-independent ( $m_F = 0$ ) spin projections, which are of great interest for many precision experiments [5], cannot be confined in magnetic traps.

Far-detuned optical dipole traps can confine atoms in arbitrary spin states. Dipole traps furthermore allow for very variable trapping geometries, as, e.g., periodic lattice geometries. Experiments aiming at achieving quantum degeneracy in optical dipole traps were first carried out by the Stanford group [7]. In far-detuned dipole traps, a variety of refined optical and evaporative cooling techniques have been implemented, which has allowed for atomic phase space densities very close to quantum degeneracy [6]. Friebel et al. found that in quasi-static dipole traps, as can be realized with a CO<sub>2</sub> laser, polarization gradient cooling alone can accumulate atoms to a phase space density three orders of magnitude above that of a conventional MOT [8]. Chapman and coworkers have reported the observation of Bose–Einstein condensation by direct evaporative cooling in a crossed CO<sub>2</sub>-laser dipole trap [10]. All-optical cooling techniques have also enabled the first observations of quantum degeneracy of <sup>6</sup>Li, cesium, and ytterbium atoms [11–13].

We here describe experiments creating rubidium Bose–Einstein condensates by direct evaporative cooling in both a crossed- and a single-beam quasi-static dipole-trapping geometry [14]. Due to the choice of a tight trapping laser focus, stable evaporation to a Bose–Einstein condensate is possible in both geometries even with a moderate initial number of atoms. The single dipole trapping geometry, in particular, allows for a considerable experimental simplification of methods for producing Bose-condensed atoms. Note that previous experiments realizing quantum degeneracy in dipole traps have either required a more alignment-sensitive crossed-beam geometry or Feshbach resonances to enhance the collisional rate [10–13]. By applying a magnetic field gradient to the single-beam configuration, we realized a trap stable for atoms in a field-insensitive  $m_F = 0$  spin projection only. In a recent work, this enabled us to realize an all-optical atom laser [15]. The chemical potential of the generated condensate is first order insensitive to fluctuations from stray magnetic fields.

## 2 Quasi-static optical dipole traps

Optical dipole traps for atoms are based on the force that arises from the coherent interaction between the induced atomic dipole moment and the laser electric field [17, 18]. When the laser frequency is tuned to the red side of an atomic resonance, the dipole force pulls atoms towards

✉ Fax: +49-7071/29-5829,  
E-mail: cennini@pit.physik.uni-tuebingen.de

the intensity maxima of the field. For optical fields with frequencies far below all electric dipole resonances of ground state atoms (i.e. ‘quasi-static’ fields), the trapping potential is given by

$$U = -\frac{1}{2}\alpha_s |\vec{E}|^2, \quad (1)$$

where  $\alpha_s$  denotes the static atomic polarizability of the electronic ground state and  $E$  is the electric field of the optical wave. For the ground state and the first excited state of the rubidium atom, the scalar static polarizability is  $\alpha_{5P} = 5.3 \times 10^{-39} \text{ m}^2 \text{ C/V}$  and  $\alpha_{5P} = 1.3 \times 10^{-38} \text{ m}^2 \text{ C/V}$ , respectively [19]. Since the frequency of the CO<sub>2</sub>-laser radiation ( $\lambda$  is near 10.6  $\mu\text{m}$ ) used in our experiment is approximately one order of magnitude below that of a typical electric dipole transition of ground state alkali atoms, the photon scattering rate is very small. In particular, the Rayleigh photon scattering rate in this quasi-static regime is given by the expression

$$\Gamma_s = \frac{16r_0^2 P}{3\hbar w_0^2} \left( \frac{m_e \alpha_s}{e^2} \right) \omega^3, \quad (2)$$

where  $w_0$  is the beam waist of the laser beam with power  $P$ ,  $r_0$  is the classical electron radius,  $m_e$  is the electron mass, and  $\omega$  denotes the optical frequency of the laser light. In our experiments, the Rayleigh scattering rate of trapped rubidium atoms is on the order of 1/600 s. This results in a small coupling of the atoms to the environment, so that the effect of decoherence can be kept small. Let us note that for alkali atoms trapped in an extremely far-detuned laser field, the detuning from resonance is much larger than both the hyperfine and fine structure splittings. This condition is met in our quasi-static trapping field. The trapping potential for ground-state alkali atoms here corresponds to that of a  $J = 0$  to  $J' = 1$  transition, and the ac Stark shift for all ground-state sublevels is almost identical. This state-independent confinement of extremely far-detuned optical dipole traps for many experiments represent an advantage over magnetic traps. It is however clear that evaporative cooling cannot be achieved by selectively transferring atoms into untrapped states, as is usually done in magnetic traps. Such a cooling in optical traps can be achieved by lowering the intensity of the trapping beams in a controlled way, which decreases the depth of the trapping potential [7].

### 3 Experimental setup and procedure

A scheme of our experimental setup used for direct Bose–Einstein condensation of rubidium atoms in a dipole trap is shown in Fig. 1. A commercial rf-excited single-mode CO<sub>2</sub> laser generated up to 50-W mid-infrared radiation near 10.6  $\mu\text{m}$ . The light passed through two acousto-optic modulators (AOMs). The first one allowed us to regulate the laser beam intensity via control of the rf-drive power. The light diffracted in first order from this modulator passed through a second AOM, whose function was that of a beam divider for the crossed-beam experiments. Note that the zeroth and first order diffracted beams differed in frequency, which eliminated unwanted standing-wave effects. The mid-infrared beams entered a vacuum chamber through ZnSe windows. For each beam, an adjustable, spherically corrected ZnSe lens

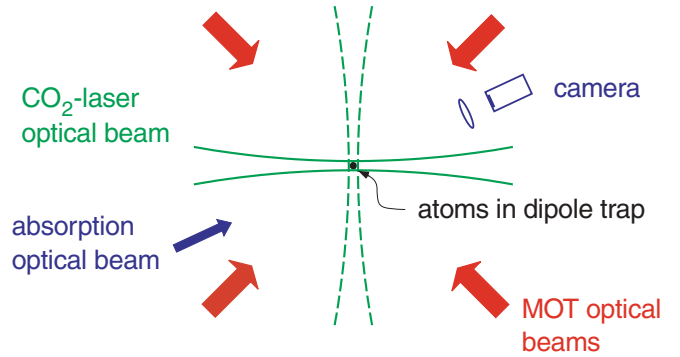


FIGURE 1 Scheme of experimental setup

( $f = 38.1 \text{ mm}$ ) placed inside the vacuum chamber focused the laser beams to a minimum waist size of 20  $\mu\text{m}$ . The beam focus could be varied with a telescope located outside the vacuum chamber. For the crossed trap geometry, a beam waist of 35  $\mu\text{m}$  was chosen, whereas for the single running wave geometry we used a beam size of 27  $\mu\text{m}$  in the trapping region. For the former geometry, the trapping beams were directed horizontally and vertically, respectively, and crossed each other at an angle of 90 degrees. For the single-beam trapping geometry, the second AOM was omitted and the transmitted beam traveled through the vacuum chamber in a horizontal direction.

Atoms of the isotope <sup>87</sup>Rb were initially collected and pre-cooled in a magneto-optical trap (MOT), which was loaded from the thermal gas emitted by heated rubidium dispensers. The measured background gas pressure inside the vacuum chamber was 10<sup>-10</sup> mbar. The near-resonant radiation for cooling and trapping atoms in the MOT was generated by grating-stabilized diode lasers. A cooling laser was operated with variable red detuning from the closed  $5S_{1/2}$ ,  $F = 2$  to  $5P_{3/2}$ ,  $F' = 3$  hyperfine component of the rubidium  $D2$  line. Its radiation was amplified by a second injection locked free-running diode laser. In order to repump rubidium atoms into the cooling cycle, a second grating-stabilized diode laser locked to the  $5S_{1/2}$ ,  $F = 1$  to  $5P_{3/2}$ ,  $F' = 2$  transition was employed. Both cooling and repumping light beams passed through acousto-optic modulators and were spatially filtered. These near-resonant beams were expanded to a beam diameter of 20 mm, spatially overlapped, and then directed into the vacuum chamber to provide three retroreflected MOT beams. The total optical power of the cooling light after spatial filtering was 42 mW, whereas that of the repumping light was 9 mW. We used a pair of magnetic coils oriented in an anti-Helmholtz configuration to generate a magnetic quadrupole field with a 10-G/cm field gradient, whose center was close to the intersection of the two CO<sub>2</sub>-laser beams. The coil axes were oriented at an angle of 45 degrees with respect to the vertical and horizontal CO<sub>2</sub>-laser beams. This quadrupole field was, e.g., used to operate the MOT.

An experimental cycle began by loading the magneto-optical trap. During the course of the experiment, we used different MOT loading times. A typical value for, e.g., the earlier crossed-beam dipole-trapping experiments was 10<sup>7</sup> trapped atoms in the MOT accumulated during a 5-s loading time. During this MOT loading phase, the cooling laser operated with a red detuning of 18 MHz to the red of the cycling tran-

sition. Subsequently, we increased the detuning of the cooling laser to a value of 160 MHz and simultaneously reduced the repumping laser intensity by a factor 100 for a 60-ms-long time interval. In this temporal dark MOT phase (d-MOT) [20], the atoms were pumped into the lower hyperfine state ( $F = 1$ ), which reduced hyperfine-changing collisions. These quoted parameters were optimized by maximizing the number of atoms transferred to the dipole trap. Throughout this cycle the CO<sub>2</sub>-laser radiation was left on, allowing for rubidium atoms to accumulate in the dipole-trapping region. At the end of the d-MOT phase, the repumping light was extinguished and after a delay of 2 ms so was the cooling light. Simultaneously, the magnetic quadrupole field was switched off. By this time, the atoms were confined by the quasi-static dipole trap alone. All near-resonant beams were carefully extinguished by both AOMs and mechanical shutters. The small delay between the extinguishing of the repumping and cooling light minimized losses in the dipole trap due to hyperfine-changing collisions.

To analyze the properties of the trapped atomic clouds, we employed the technique of absorption imaging. At the end of an experimental cycle, the trapped atoms were released by switching off the CO<sub>2</sub>-laser beams. After a variable expansion time (typically 5–20 ms), cold atoms were irradiated with a pulse of light tuned resonantly to the  $F = 2$ ,  $F' = 3$  component of the rubidium  $D2$  line. For this measurement, we used a spatially filtered laser beam with a beam diameter of 8 mm. The beam was then imaged onto a slow-scan CCD camera, where shadow images of the atomic cloud were recorded. From these images, both the number of atoms and atomic temperatures were extracted. The pulse length was 80  $\mu$ s and the intensity (100  $\mu$ W/cm<sup>2</sup>) was chosen to be clearly below saturation intensity. During this detection time, repumping light was provided by the MOT beams.

## 4 Experimental results

### 4.1 Bose–Einstein condensation in a crossed-beam geometry

In initial experiments, we studied BEC in a crossed-beam geometry, in a similar fashion to work done by Chapman

et al. [10]. To reach Bose–Einstein condensation by direct evaporative cooling in our dipole traps, the initial phase space density of the laser-cooled clouds was first optimized. We characterized the trap lifetime, trap frequencies, and temperature of the trapped atomic cloud. The vibrational frequencies were measured by periodically modulating the optical confining power with the first AOM, which allowed us to parametrically study excitation of the trapped atoms [21]. Significant trap loss was observed when the modulation frequency was close to twice a trap vibrational frequency. With typical parameters of 12 W of optical power in each of the CO<sub>2</sub>-laser trapping beams and a 35- $\mu$ m waist radius, we observed parametric resonance corresponding to a vibrational frequency of  $\nu = 1.7$  kHz. For this crossed-beam geometry, the oscillation frequencies in the central trap region in all three spatial directions were similar. The trap lifetime was extracted by monitoring the number of atoms detected after different trapping times for a constant potential depth. A typical result of such a measurement is shown in Fig. 2a. The data points were taken after a minimum dipole-trapping time of 70 ms, since for shorter delay times atoms not transferred to the dipole trap have not yet been removed completely from the detection region by gravity. The data can be described by a two-time-constant exponential decay, which involves a fast and a slow decay with time constants near 100 ms and 12 s, respectively. The fast decay in the beginning of the dipole-trapping phase is attributed to a plain atomic evaporation of the most energetic atoms. In contrast, the slow decay is attributed to losses due to collisions with the background gas, which ultimately limit the available trapping time. Figure 2b shows the dependence of the atomic temperature on the trapping time. The temperature clearly decreases with time, which we attribute to the plain evaporation. This process is effective only for small trapping times when the loss rate is large. The measured atomic density after a trapping time of 500 ms was  $10^{13}$  atoms/cm<sup>3</sup>. Together with the measured temperature of 60  $\mu$ K we derived a phase space product  $n\lambda_{\text{dB}}^3 \simeq 1/500$ , which corresponds to a 1/1500 phase space density if we assume an equal distribution of spin projections. These results are comparable to previous results observed in CO<sub>2</sub>-laser optical lattice and crossed dipole ge-

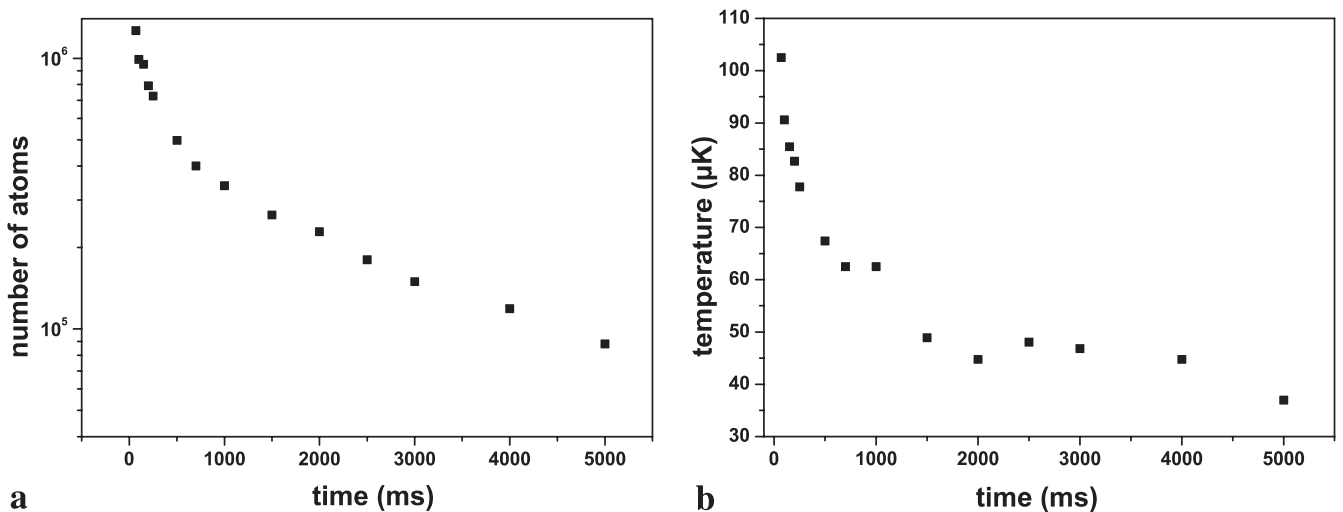


FIGURE 2 a Number of trapped atoms and b atomic temperature versus trapping time in a CO<sub>2</sub>-laser crossed dipole trap configuration

ometries [8]. We also inferred a collisional rate of 7 kHz at this time, which clearly represents a favorable starting point for further, forced evaporative cooling to lower temperatures. To induce such a forced evaporation, the optical potential was lowered in a controlled way. Experimentally, this was achieved by reducing the trapping laser beam intensity via a decrease in the rf-drive power of the first AOM. Mandatory for the success of evaporative cooling is maintaining a relatively high atomic collision rate, so that the remaining atoms can rethermalize to a distribution of lower temperature. We reduced the potential depth with time according to the formula

$$U(t) = U_0(1 + t/\tau)^{-\beta}, \quad (3)$$

where  $U_0$  denotes the value of the initial potential depth. It was shown in [9] that this ramp form maintains a nearly constant ratio  $\eta = U/k_B T$  between the potential depth and the atomic temperature. Following a 100-ms-long plain evaporation period, the mid-infrared power was reduced in a 3.5-s-long ramp time from 12 W initially to a final value of 75 mW in each of the trapping beams. In these crossed dipole experiments, we found optimum cooling when the parameters of (3) were chosen to be  $\tau = 0.3$  s and  $\beta = 1.5$ . We experimentally verified that the cutoff parameter  $\eta$  was nearly constant throughout the evaporation ramp. To characterize the cooling, we analyzed shadow images of the expanded atomic cloud at the end of the evaporation process. Figure 3a shows a cross-section of such an image for a final trapping power of 150 mW, which corresponds to an average trap vibrational frequency of 350 Hz. It is clear that the ensemble here was still purely thermal. The phase space density was further increased when we ramped to lower power values. Figure 3b shows data recorded for a final beam power of 100 mW, for which a typical bimodal distribution corresponding to an atomic cloud near the transition point was observed. The central feature corresponds to atoms in the Bose condensate, while the wings represent thermal atoms. The critical temperature here was  $T_c = 190$  nK. For a final power of 75 mW, an almost pure condensate was obtained as shown in Fig. 3c. The condensate contained about 10 000 atoms distributed among the three

$m_F$  states of the electronic hyperfine ground state  $F = -1$ . In other measurements, we applied a magnetic quadrupole field during the course of the evaporation by leading on the MOT coils. This led to a condensate with about 70% population in the  $m_F = 1$  and 30% in the  $m_F = 0$  spin projection. For these trap parameters, the magnetic field gradient predominantly populated one field-sensitive state. In earlier work in a crossed dipole trap it was demonstrated that with different field gradients other spin states can also be populated, although by the time of writing the origin of the obtained magnetization still remained to be determined [16].

#### 4.2 BEC in a single running wave trap

In this section, we describe our experiments in which a rubidium Bose–Einstein condensate was successfully created in a single-beam CO<sub>2</sub>-laser dipole trap. This is the simplest possible dipole trapping geometry. The use of single running wave allows for a compact setup and a very reliable production of the BEC. Previous experiments creating quantum degeneracy in dipole traps have either required the use of a more alignment-sensitive crossed dipole trap geometry [10, 13] or Feshbach resonances [12] to enhance the collisional rate during the course of the forced evaporation.

As in the case of the crossed dipole trap configuration, evaporative cooling towards BEC requires a ramping down of the trapping potential. Since the average of the trap vibrational frequencies for a given power and beam waist is smaller than in the crossed-beam geometry, it is not clear a priori that the rethermalization rate is sufficiently high throughout the evaporation ramp. Obviously, the final stages of evaporation here are most critical, since the collisional rate decreases with trap power. It is easy to show that the trap vibrational frequencies in a single dipole trap orthogonal to the beam axis scale as  $\nu_r \propto \sqrt{P}/w_0^2$ , while along the beam axes scale as  $\nu_z \propto \lambda\sqrt{P}/w_0^3$ , where  $\lambda$  is the laser wavelength. Our experiments demonstrate that by choosing a sufficiently small beam waist, the collisional rate can be high enough throughout the ramp, and BEC can be reached. For the single-beam geometry, the focus of the (horizontally oriented) trapping beam

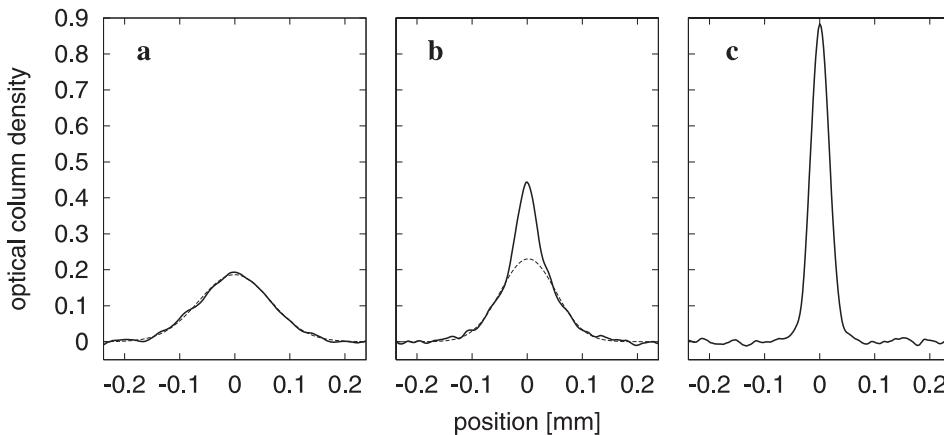


**FIGURE 3** Formation of a Bose–Einstein condensate in a crossed-beam dipole trap. The plots show density profiles for several values of the final trapping-beam power. **a** 150 mW, which yields a thermal cloud corresponding to a temperature of 240 nK. 100 mW, which yields an atomic temperature of 200 nK. This value is near the critical temperature of 190 nK. A bimodal distribution with the central feature corresponding to Bose-condensed atoms and a thermal atomic distribution in the wings is visible. **c** 75 mW. An almost pure Bose–Einstein condensate is produced

was reduced to a beam waist of 27  $\mu\text{m}$ . In principle, one could work with an even tighter focus to fully compensate for the smaller compression in this geometry. In our experiments, we instead started with a larger number of atoms and also used a slightly longer evaporation time. The weak confinement along the beam axis of the single dipole trap geometry offers the additional benefit that it allows us to remove atoms in field-sensitive spin projections with a moderate magnetic field gradient. We note that an alternative to such a state selection is to achieve field insensitivity by using atoms with a spin singlet ground state, such as, e.g., atomic ytterbium. Very recently, in an impressive experiment, evaporative cooling in a crossed dipole trap allowed for the production of a Bose–Einstein condensate of these atoms [13].

For our single dipole trap experiments, we increased the MOT loading time to 30 s, during which  $6 \times 10^7$  were captured. At the end of the MOT loading, we applied a temporal dark MOT phase as described in the above section. Subsequently, all near-resonant optical beams were extinguished and the atoms were trapped in the quasi-static dipole-trapping potential alone. Typically,  $4 \times 10^6$  atoms were captured in the single-beam trap. We characterized the vibrational frequencies of the trap. At a full trapping laser power (28 W), we measured  $\nu_r = 4.8$  kHz and  $\nu_z = 350$  Hz, corresponding, respectively, to vibrations orthogonal and collinear to the beam axes. In this single-beam geometry, there was no spherical symmetry and the longitudinal trap frequency was about 13 times smaller than the radial one. Again, we first analyzed the trapping of atoms while maintaining full CO<sub>2</sub>-laser trapping power. Following a 100-ms-long plain evaporation phase, we measured an atomic temperature of 140  $\mu\text{K}$  and an atomic density of  $n \simeq 1.2 \times 10^{13}$  atoms/cm<sup>3</sup>. This corresponds to a product  $n\lambda_{\text{dB}}^3 \simeq 1.2 \times 10^{-4}$ . Although this value is below the best values obtained in quasi-static crossed dipole trap configurations or optical lattices, it is clearly above results achieved in magnetic traps prior to forced evaporative cooling. From the above values, we derived a high collision rate of 6.2 kHz, which encouraged us to proceed with forced evaporative cooling in this single-beam dipole-trapping geometry.

To cool the atoms towards lower temperatures, we applied a 7-s-long forced evaporation ramp, during which the power of the dipole-trapping beam was reduced from its initial value of 28 W to a final value of 200 mW. This ramp was applied directly after the dark MOT phase, since for this geometry no

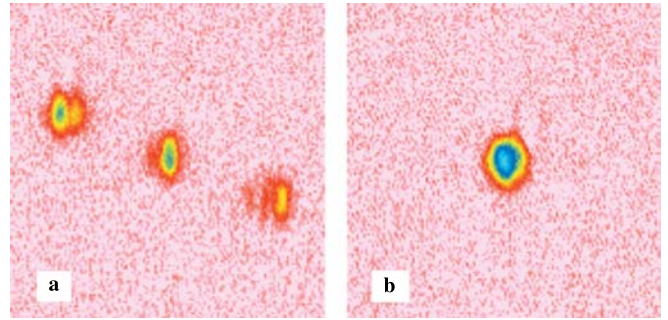


**FIGURE 4** Free expansion of a Bose–Einstein condensate generated in a single-beam dipole trap. Shown is a series of shadow images of the atomic cloud recorded after allowing for different free expansion times (field of view  $240 \mu\text{m} \times 240 \mu\text{m}$ ). **a** Image taken with nearly no free expansion, thus showing the cigar-shaped spatial distribution of the trapped cloud. **b** and **c** Recorded after 8 ms and 15 ms, respectively, of free expansion. The asymmetry of the cloud is inverted especially at the latter time

improved cooling was observed when an initial plain evaporation phase is added. We again used a ramp form as described by (3). Optimum cooling in the single dipole trap was observed when using parameters  $\tau$  and  $\beta$  near 0.45 s and 1.4, respectively. We recorded time-of-flight (TOF) shadow images of the atomic cloud for different free expansion times. For this measurement, the MOT quadrupole field was switched off after the d-MOT phase. Figure 4a shows an image recorded directly after switching of the trap laser, i.e., with no free expansion. The trapped cloud is cigar shaped and strongly elongated along the weakly confining beam axis. Figure 4b and c give time-of-flight images recorded after a free expansion phase of 8 and 15 ms, respectively. In the former image the cloud is almost symmetric, while in the latter image the symmetry axis is inverted. We interpret this series of images as clear evidence for Bose–Einstein condensation in the single-beam optical trap. In this asymmetric trap geometry, the cloud expands faster along the radial than along the axial direction due to the anisotropic release of mean field energy. The formed condensate has spinor nature. To analyze the distribution of Zeeman components, we applied a Stern–Gerlach magnetic field gradient during the free expansion phase, which spatially separates the different Zeeman components. Figure 5 a shows a typical measurement, in which a separation into clouds with different spin projections is clearly visible. We produced condensates with typically 12 000 atoms distributed among

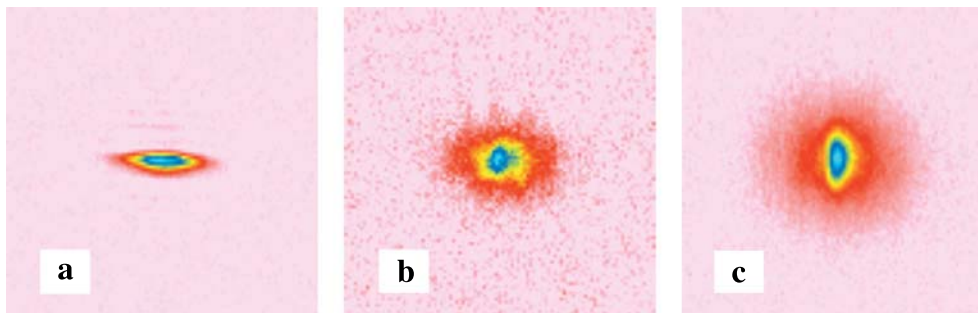


**FIGURE 5** Shadow images of Bose–Einstein condensates generated in a single-beam dipole trap after allowing 15 ms of free expansion (see also [15]). The field of view comprises  $380 \mu\text{m} \times 380 \mu\text{m}$ . **a** Stern–Gerlach magnetic field applied only during the free expansion phase. The three components  $m_F = \pm 1, 0$  of a spinor condensate have separated into three spatially resolved clouds. **b** Stern–Gerlach field activated during the evaporative cooling phase. Here, a pure  $m_F = 0$  condensate is generated

the  $m_F = -1, 0, 1$  Zeeman components of the  $F = 1$  ground state. As stated above, one of the main advantages of optical dipole traps is their state-independent trapping, which allows for the formation and confinement of spinor condensates.

In subsequent experiments, we condensed atoms in the  $m_F = 0$  spin projection only. For this measurement, the magnetic quadrupole field generated by the MOT coils was left on throughout the experimental cycle, i.e., during both dipole-trapping and detection phases. For our experimental parameters, stable trapping of atoms during the final phase of the evaporative cooling was then only possible for the field-insensitive ( $m_F = 0$ ) spin projection. Atoms in spin projections  $m_F = \pm 1$  were removed during the course of evaporative cooling by the field gradient (note that the dipole trap does in general not exactly overlap with the center of the quadrupole field). Figure 5b shows a typical time-of-flight shadow image of the condensed cloud that was obtained. The measurement shows that only the  $m_F = 0$  Zeeman state was populated. We typically obtained 7000 condensed atoms in this first order field-insensitive state. Note that this number is larger than the obtained  $m_F = 0$  fraction of the above discussed spinor condensate, which we attribute to sympathetic cooling with atoms in  $m_F = \pm 1$  spin projections during condensate formation. The critical temperature of the  $m_F = 0$  condensate was  $T_c \simeq 220$  nK, and the peak-density was  $1.2 \times 10^{14} / \text{cm}^3$ . For both the spinor and the  $m_F = 0$  condensate we measured condensate lifetimes near 5 s. This value is shorter than the inverse loss rate due to background gas collisions, and we attribute this lifetime to be mainly limited by three-body losses. Within our experimental uncertainty, we did not observe any difference between the lifetimes of a spinor and the  $m_F = 0$  condensate. Furthermore, we did not observe transfer of atoms from  $m_F = 0$  state into field-sensitive states. To our belief, spin-changing collisions here were suppressed by the quadratic Zeeman shift in the inhomogeneous magnetic field [22, 23].

## 5 Conclusions and outlook

We have investigated Bose–Einstein condensation of rubidium atoms by direct evaporative cooling in tightly confining, quasi-static dipole traps. The quantum degenerate regime was reached both in a crossed-beam and a single-beam CO<sub>2</sub>-laser dipole-trapping geometry. The former configuration allows cooling to quantum degeneracy with a somewhat larger trap focus. On the other hand, the newly developed single-beam approach towards Bose–Einstein condensation provides a simpler setup and is less alignment sensitive. The scheme provides a very stable route towards the achievement of quantum degeneracy. Finally, we have demonstrated that in the single-beam setup a moderate magnetic field gradient yields a trapping configuration, in which stable confinement is possible only for atoms in an  $m_F = 0$  spin projection. The chemical potential of the produced Bose–Einstein condensate is first order insensitive to stray magnetic fields.

For the future, we believe that the demonstrated single-beam method for producing Bose–Einstein condensates, due to its technical simplicity, opens up the possibility of diverse applications in the physics of quantum gases. Further research could investigate an extension to the Bose–Einstein conden-

sation of other atomic species, such as, e.g., alkaline-earth atoms.

Furthermore, we anticipate that the method described for producing condensates in a field-insensitive spin state will have an impact on the application of quantum degenerate atoms to precision measurements, such as those of, e.g., atomic clocks or atom interferometry experiments. One can furthermore envision experiments with two-component quantum degenerate gases driven by excitation of the microwave clock transition between the hyperfine ground states  $F = 1, m_F = 0$  and  $F = 2, m_F = 0$ . It clearly remains important to study the stability of different spin projections against spin-changing collisions in more detail.

Quasi-static optical dipole traps are of great interest for quantum computation. In a CO<sub>2</sub>-laser lattice geometry the lattice spacing is so large that individual sites can be optically resolved, which allows for an individual addressing of qubits [24]. By inducing a Mott-insulator phase transition, unity occupation of atoms in lattice sites can be achieved. An entanglement of atoms in the lattice is, e.g., possible by cold, controlled collisions [25].

**ACKNOWLEDGEMENTS** This work has been supported in part by the Deutsche Forschungsgemeinschaft, the Landesstiftung Baden Württemberg, and the European Community.

## REFERENCES

- 1 E.A. Cornell, C.E. Wieman: *Rev. Mod. Phys.* **74**, 875 (2002)
- 2 W. Ketterle: *Rev. Mod. Phys.* **74**, 1131 (2002)
- 3 F. Dalfovo, S. Giorgini, L.P. Pitaevskii, S. Stringari: *Rev. Mod. Phys.* **71**, 463 (1999)
- 4 M. Greiner, O. Mandel, T. Esslinger, T.W. Hänsch, I. Bloch: *Nature* **415**, 39 (2002)
- 5 P. Gill: *Frequency Standards and Metrology* (World Scientific, Singapore 2002)
- 6 A.J. Kerman, V. Vuletić, C. Chin, S. Chu: *Phys. Rev. Lett.* **84**, 439 (1999); D.J. Han, S. Wolf, S. Oliver, C. McCormick, M.T. DePue, D.S. Weiss: *Phys. Rev. Lett.* **85**, 724 (2000); T. Ido, Y. Isoya, H. Katori: *Phys. Rev. A* **61**, 061403 (R) (2000)
- 7 C.S. Adam, H. Jin Lee, N. Davidson, M. Kasevich, S. Chu: *Phys. Rev. Lett.* **74**, 3579, (1995)
- 8 S. Friebel, R. Scheunemann, J. Walz, T.W. Hänsch, M. Weitz: *Appl. Phys. B* **67**, 699 (1998)
- 9 R. Grimm, M. Weidemüller, Y.B. Ovchinnikov: *Adv. At. Mol. Opt. Phys.* **42**, 95 (2000)
- 10 M.D. Barrett, J.A. Sauer, M.S. Chapman: *Phys. Rev. Lett.* **87**, 010404 (2001)
- 11 S.R. Granade, M.E. Gehm, K.M. O'Hara, J.E. Thomas: *Phys. Rev. Lett.* **88**, 120405 (2002)
- 12 T. Weber, J. Herbig, M. Mark, H.C. Nägerl, R. Grimm: *Science* **299**, 232 (2003)
- 13 Y. Takasu, K. Maki, K. Komori, T. Takano, K. Honda, M. Kumakura, T. Yabuzaki, Y. Takahashi: *Phys. Rev. Lett.* **91**, 0404041 (2003)
- 14 Our crossed dipole work was first reported at the 67. Physikertagung und AMOP-Frühjahrstagung, Hannover 2003; see also: G. Cennini, G. Ritt, C. Geckeler, M. Weitz: *Verhandl. DPG (VI)* **38**, (2003)
- 15 G. Cennini, G. Ritt, C. Geckeler, M. Weitz: *cond-mat/0307620*
- 16 M.D. Barrett, M.S. Chang, C. Hamely, K. Fortier, J.A. Sauer, M.S. Chapman: In: "Proc. XVIII Int. Conf. Atomic Physics", ed. by H.R. Sagehpour, E.J. Heller, D.E. Pritchard (World Scientific, 2003)
- 17 S. Chu, J.E. Bjorkholm, A. Ashkin, A. Cable: *Phys. Rev. Lett.* **57**, 314 (1985)
- 18 C. Cohen-Tannoudji: "Atomic Motion In Laser Light". In: *Les Houches, Session LIII, 1990*, ed. by J. Dalibard, J.M. Raimond, J. Zinn-Justin (North Holland, Amsterdam 1992)
- 19 D.R. Lide: *CRC Handbook of Chemistry and Physics* (CRC Press, Boca Raton 1990); R. Marrus, D. McColm, J. Jellin: *Phys. Rev.* **147**, 55 (1966)
- 20 W. Ketterle, K.B. Davis, M.A. Joffe, A. Martin, D.E. Pritchard: *Phys. Rev. Lett.* **70**, 2253 (1997)

- 
- 21 S. Friebel, C. D'Andrea, J. Walz, M. Weitz, T.W. Hänsch: Phys. Rev. A **57**, R20 (1998)
- 22 N.N. Klausen, J.L. Bohn, C.H. Greene: Phys. Rev. A **64**, 053602 (2001); E.G.M. van Kempen, S.J.J.M.F. Kokkelmans, D.J. Heinzen, B.J. Verhaar: Phys. Rev. Lett. **88**, 093201 (2002)
- 23 R. Grimm: private communication
- 24 R. Scheunemann, F.S. Cataliotti, T.W. Hänsch, M. Weitz: Phys. Rev. A **62**, 51801 R (2000)
- 25 D. Jaksch, H.-J. Briegel, J.I. Cirac, C.W. Gardiner, P. Zoller: Phys. Rev. Lett. **82**, 1975 (1999)